Microfibrillar Network of a Rigid Rod Polymer. 2. Small-Angle X-ray Scattering

Yachin Cohen† and Edwin L. Thomas*

Polymer Science and Engineering Department, University of Massachusetts, Amherst, Massachusetts 01003. *Received February 23, 1987*

ABSTRACT: The network of oriented microfibrils, which is formed in the coagulation stage of the spinning process of poly[*p*-phenylene(benzo[1,2-*d*:4,5-*d'*]bisthiazole-2,6-diyl)] (PBT) fibers and films, is characterized by small-angle X-ray scattering (SAXS) measurements. PBT films, processed by uniaxial extrusion and coagulation in water, are impregnated with an epoxy resin. SAXS measurements are performed by using a slit-collimated incident beam. The scattering pattern obtained reflects the structure in a cross-section plane perpendicular to the extrusion direction. The theoretical framework for the analysis of such patterns in terms of the scattering from two-dimensional structures is outlined. It allows the calculation of the average width (71 Å), density (1.46 g/cm^3), and volume fraction (18%) of the microfibrillar PBT phase in the epoxy impregnated film. The scattering pattern is simulated by using three structural models for the spatial arrangement of the microfibrillar cross sections: a "fluidlike" system of hard disks, a similar system of semipenetrable disks, and a random two-phase structure. The latter model exhibits the best fit of the measured pattern, implying that the microfibrils have irregularly shaped cross sections.

Introduction

Many systems, both of natural and of synthetic origin, which are formed in a uniaxial process, exhibit a morphology which is fibrillar in nature. Some examples are synthetic fibers,[1] craze fibrils formed in glassy polymers under uniaxial tension,[2,3] and chitin microfibrils in certain parts of the cuticle of insects.[4] In a previous study of high-performance fibers and films made from a rigid polymer poly[*p*-phenylene(benzo[1,2-*d*:4,5-*d'*]bisthiazole-2,6-diyl)],[5] we have shown that the structure formed in the coagulation stage of the solution spinning process is a network of oriented microfibrils, with a typical width of about 100 Å. The microfibrils constitute the basic structural elements of the fiber. Visualization by electron microscopy of regions buckled under compression[5] has indicated that it is the buckling of the individual microfibrils that is responsible for the compressive failure of the material. The compressive strength should therefore be sensitive to the ratio of the width to length of the microfibril, whenever failure occurs by buckling.[5] A quantitative measure of the microfibrillar morphology in such oriented systems is thus important.

Estimates of the microfibrillar width have been obtained by a variety of methods. Electron microscopy allows for direct visualization whenever sufficiently thin samples can be obtained. A lower bound of the diameter of crystalline microfibrils can be estimated from line-broadening studies of equatorial wide-angle X-ray diffraction (WAXD) peaks. Small-angle X-ray scattering (SAXS) can also be used to study the width of microfibrils, using both pinhole and slit-collimated incident beams.

The objectives of this study are (a) to outline the relations which allow the interpretation of SAXS patterns obtained from oriented fibrillar systems with a slit-collimated incident beam and (b) to use these relations for a quantative measure of the microfibrillar morphology formed in the coagulation stage of the processing of poly[*p*-phenylene(benzo[1,2-*d*:4,5-*d'*]bisthiazole-2,6-diyl)] (PBT) films. SAXS measurements will thus provide complementary information to that obtained by direct visualization using electron microscopy,[5] especially with regards to the microfibrillar cross sections which could not be observed successfully.[5]

† Current address: Chemical Engineering Department, Technion, Haifa, Israel.

Experimental Section

PBT (inherent viscosity of 18 in methanesulfonic acid, for which a molecular weight of approximately 35 000 is estimated[6]) was obtained from J. Wolfe of SRI as a 5.6% (w/w) solution in poly(phosphoric acid), its polymerization medium.[7] Films were spun from this solution by extrusion through a 1-mm-wide rectangular die. The extrudate was extended 3 times in an air gap, coagulated in a water bath, and kept subsequently under water. The wet films were impregnated with an epoxy resin as described previously,[5,8] in order to minimize changes in the microstructure of the coagulated state that would have occurred during drying.

Small-angle X-ray scattering (SAXS) patterns from a pinhole collimated incident beam were obtained with a Statton camera and recorded on flat film. The sample to film distance was 313 mm. The SAXS pattern from a slit-coillimated incident beam was obtained with a Kratky camera and recorded electronically by using a Braun position-sensitive detector. The film was placed with the extrusion direction parallel to the direction of the collimation slit. The sample to detector distance was 531 mm. The scattered intensity was measured in absolute units by using a Lupolen calibration standard.[9] In both cases Cu Kα radiation was used.

Analysis of a Scattering Pattern Obtained by Using a Slit-Collimated Incident Beam

The analysis of the scattering pattern obtained from an oriented fibrillar system by using a slit-collimated incident beam has been discussed by Perret and Ruland[10] and Dettenmaier,[11] but details of the derivation of the scattering laws have not been published. These derivations[12] follow the classical treatment of Porod,[13] Debye and Bueche,[14] and Debye, Anderson, and Brumberger,[15] for the scattering from an isotropic system from a pinhole-collimated incident beam. A similar derivation has been used by Kirste and Porod[16] for the analysis of the scattering from "infinitely long" structures. The theoretical framework for the analysis of SAXS patterns obtained from oriented systems by using a slit-collimated incident are outlined below, with emphasis on the limits of its validity.

The scattering pattern obtained from a pinhole-collimated incident beam is the Fourier transform of the electron density correlation function:[13,14]

$$I(\mathbf{s}) = \langle \eta^2 \rangle \int_{-\infty}^{\infty} \gamma(\mathbf{r}) e^{i(2\pi \mathbf{s}\cdot\mathbf{r})}\, d\mathbf{r}^3 \qquad (1)$$

where $I(\mathbf{s})$ is the absolute scattered intensity per unit volume (electrons^2/cm^3), $\mathbf{r}(x_1,x_2,x_3)$ is a spatial position vector, $\mathbf{s}(s_1,s_2,s_3)$ is a vector in reciprocal space for which $|s| = 2 \sin\theta/\lambda$, where 2θ is the scattering angle and λ is the

0024-9297/88/2221-0436$01.50/0

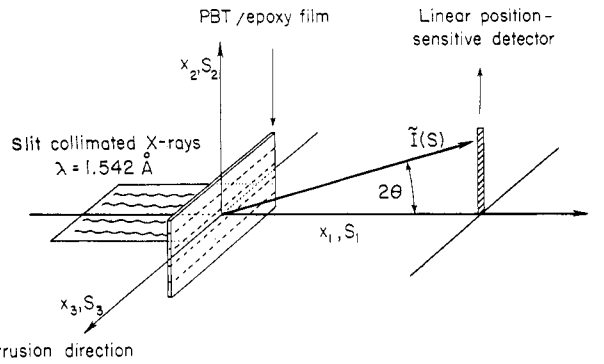

Figure 1. Geometry of the small-angle X-ray scattering experiment.

wavelength of radiation. $\gamma(\mathbf{r})$ is the correlation function, defined as[14]

$$\gamma(\mathbf{r}) = \langle \eta(\mathbf{r}' + \mathbf{r})\eta(\mathbf{r}') \rangle_{\mathbf{r}'} / \langle \eta^2(\mathbf{r}') \rangle_{\mathbf{r}'} \quad (2)$$

where $\eta(\mathbf{r})$ is the fluctuation in electron density $\rho(\mathbf{r})$:

$$\eta(\mathbf{r}) = \rho(\mathbf{r}) - \langle \rho(\mathbf{r}') \rangle_{\mathbf{r}'} \quad (3)$$

The geometry of a small-angle scattering experiment using a slit-collimated incident beam is shown in Figure 1, where the x_3 axis defines the direction of the collimation slit. The scattered intensity measured at position P on the detector is the sum of contributions from all volume elements of the sample irradiated by the beam. Analysis of the scattering pattern obtained under such conditions is simplified if the following assumptions are met:

(a) The slit-collimated beam incident on the sample can be assumed to be of infinite length. This assumption is valid if the scattered intensity in the s_3 direction decays to a negligible level for scattering vectors s_3 which are much smaller than a critical value of $S^* = x^*_3/L\lambda$, where L is the sample to detector distance and x^*_3 is the value of x_3 up to which the beam incident on the sample is of constant intensity.

(b) The structure is homogeneous in the x_3 direction, such that in all cross-section planes perpendicular to the x_3 direction the structures are equivalent, having the same correlation function.

Under the approximations given above, the absolute smeared intensity per unit volume, $\tilde{I}(\mathrm{P})$ (electron^2/cm^2), is given by

$$\tilde{I}(\mathrm{P}) = \int_{-\infty}^{\infty} I(P)\, dx_3 = L\lambda \int_{-\infty}^{\infty} I(s_1,s_2,s_3)\, ds_3 \quad (4)$$

where the scattering vector s_3 has been approximated as $s_3 \approx x_3/L\lambda$.

The correlation function in a cross-section plane perpendicular to the x_3 axis is obtained by an inverse Fourier transform of eq 1, substituting $x_3 = 0$:

$$\gamma(x_1,x_2,0) = (1/\langle \eta^2 \rangle) \int\int_{-\infty}^{\infty} \left[\int_{-\infty}^{\infty} I(s_1,s_2,s_3)\, ds_3 \right] e^{-i2\pi(s_1x_1+s_2x_2)}\, ds_1\, ds_2 \quad (5)$$

Substituting (4) in (5) and Fourier inversion yield

$$\tilde{I}(\mathbf{S}) = L\lambda\langle \eta^2 \rangle \int_{-\infty}^{\infty} \gamma(\mathbf{R}) e^{i(2\pi \mathbf{S}\cdot\mathbf{R})}\, d\mathbf{R}^2 \quad (6)$$

where $\mathbf{R}(x_1,x_2)$ and $\mathbf{S}(s_1,s_2)$ are vectors in a cross-section plane perpendicular to x_3 and s_3, respectively. For a structure having cylindrical symmetry about the x_3 axis, eq 6 becomes[17]

$$\tilde{I}(S) = L\lambda\langle \eta^2 \rangle \int_0^{\infty} \gamma(R) J_0(2\pi SR) 2\pi R\, dR \quad (7)$$

where $R = |\mathbf{R}|$, $S = |\mathbf{S}|$, and J_0 is the first-order Bessel function.

Thus the slit-smeared scattering pattern is shown to be equivalent to the scattering pattern of a two-dimensional system, the structure of which is described by the cross section of the three-dimensional correlation function in a plane perpendicular to the collimation slit. In such a case the absolute smeared intensity per unit volume of a three-dimensional structure is equivalent to the absolute intensity per unit area of a two-dimensional structure. It is therefore of interest to derive some relationships between the specimen structure and the scattering pattern for a two-dimensional system, following the treatments by Porod[13] and Debye et al.[15] for the scattering from a three-dimensional system.

The scattering invariant, Q, derived by inversion of eq 7 and substituting $R = 0$, is proportional to the mean-squared density fluctuation:[13]

$$Q = \int_0^{\infty} I(S) 2\pi S\, dS = L\lambda\langle \eta^2 \rangle \quad (8)$$

For a material consisting of two homogeneous phases, Debye et al.[15] defined four probability functions $P_{ij}(r)$, (i, j = 1, 2), as the probability that one end of a cord of length r placed at random in the material is in phase j, given that the other end is in phase i. These four probabilities can be described by a single function $f(r)$:

$$\mathbf{P}_{21}(r) = v_1 f(r) \qquad \mathbf{P}_{12}(r) = (1 - v_1) f(r)$$
$$P_{ii} + P_{ij} = 1 \quad (9)$$

where v_i is the volume fraction of phase i.

For an isotropic system, irrespective of its dimensionality, Debye et al.[15] derived the following relationships:

$$\gamma(r) = 1 - f(r) \quad (10)$$

$$P_{\mathrm{D}}(r) = 2v_1(1 - v_1)[1 - \gamma(r)] \quad (11)$$

where $P_{\mathrm{D}}(r)$ is the probability that the ends of a cord of length r are found in dissimilar phases. In addition, for a two-phase system with sharp interfaces,[15]

$$\langle \eta^2 \rangle = v_1(1 - v_1)(\rho_1 - \rho_2)^2 \quad (12)$$

For a two-dimensional system, eq 11 and 12 are still valid, with v_i now defined as an area fraction.

The probability of dissimilar ends $P_{\mathrm{D}}(r)$ can also be expressed as twice the product of the probability that one end is at a distance $0 < x < r$ from the interface and the probability that the cord has the proper orientation to intersect the interface.[15] Thus for a two-dimensional system,

$$P_{\mathrm{D}}(R) = 2\int_0^R \left(\frac{C}{A}\, dx\right)\left[\frac{\cos^{-1}(x/R)}{\pi}\right] = \frac{2CR}{\pi A} \quad (13)$$

where A is the total area of the system and C is the length of the interfacial curve within A.

Equating (11) and (13) yields, in the limit of small r,

$$C/A = -\pi v_1(1 - v_1)(d\gamma/dR)_{R=0} \quad (14)$$

Taking a Taylor expansion of $\gamma(R)$ about $R = 0$ in eq 7 and a change of variables to $u = 2\pi SR$ yields

$$\tilde{I}(S) = \frac{L\lambda\langle \eta^2 \rangle}{2\pi S^2}\left[\int_0^{\infty} uJ_0(u)\, du + \frac{\gamma'(0)}{2\pi S}\int_0^{\infty} u^2 J_0(u)\, du + \frac{\gamma''(0)}{8\pi^2 S^2}\int_0^{\infty} u^3 J_0(u)\, du + \ldots\right] \quad (15)$$

Substituting in eq 15 the value of the integrals as given

in the Appendix, and using eq 12 and 14, yields the Porod relationship for the large-angle tail of the scattering pattern from a two-dimensional structure with sharp interfaces:

$$\tilde{I}(S) = [(L\lambda/4\pi^3)(\rho_1 - \rho_2)^2 C/A]S^{-3} + \mathcal{O}(S^{-5}) \quad (16)$$

The prefactor of the S^{-3} term in equation (16) is defined as the Porod constant K_p.

If the scattering elements in the two-dimensional structure can be approximated as disks covering an area fraction v_1, their average diameter, $\bar{D}$, can be obtained from the length of the interfacial curve per unit area by using eq 8, 12, and 16

$$\bar{D} = \langle D^2 \rangle / \langle D \rangle = Q/\pi^3(1 - v_1)K_p \quad (17)$$

which is the same as that derived by Paredes and Fischer[2] for scattering by cylinders.

The correlation function that describes a random two-phase structure has been derived by Debye et al.[15] for the three-dimensional case. Similarly, the two-dimensional case is considered by evaluating the change in $P_{22}(R)$ as a result of a change δR in the cord length R. A change in $P_{22}(R)$ will occur only if the free end of R is at a distance smaller than $R \cos \Omega$ from the interface, where Ω is the angle between a given orientation of R and the normal to the interfacial curve in the vicinity of the free end of R. Thus in direct analogy to the derivation of Debye et al.[15]

$$\delta P_{22}(R) = -P_{22}(R)\frac{C}{A_2}\delta R\langle \cos \Omega \rangle + P_{21}(R)\frac{C}{A_1}\delta R\langle \cos \Omega \rangle \quad (18)$$

where A_i is the area of phase i, and $\langle \cos \Omega \rangle$ is averaged over all possible orientations of R which allow it to cross the interface upon addition of δR to its free end:

$$\langle \cos \Omega \rangle = \int_{-\pi/2}^{\pi/2} \cos \Omega \, d\Omega \Big/ \int_0^{2\pi} d\Omega = 1/\pi \quad (19)$$

Using (9), (10), and (19) in (18) yields

$$\frac{d\gamma(R)}{dR} = -\frac{C}{\pi v_1(1 - v_1)A}\gamma(R) \quad (20)$$

and

$$\gamma(R) = \exp(-R/l_c) \quad (21)$$

with the correlation length l_c given as

$$l_c = \pi v_1(1 - v_1)A/C \quad (22)$$

The form of the scattering pattern from a random two-phase structure, in two dimensions, is obtained by substitution of eq 21 and 22 in eq 7 followed by a Fourier–Bessel transform:[18]

$$\tilde{I}(S) = 2\pi v_1(1 - v_1)L\lambda(\rho_1 - \rho_2)^2 l_c^2/(1 + 4\pi^2 l_c^2 S^2)^{3/2} \quad (23)$$

where we have used eq 12 for a structure with sharp interfaces.

Results and Discussion

In the accompanying publication we describe the morphology of PBT fibers and films impregnated with an epoxy resin, as revealed by electron microscopy.[5] A network of microfibrils, having a typical width of about 100 Å and which are highly oriented along the direction of extrusion, has been observed. Our objective here is to study the structure in a cross section perpendicular to the extrusion direction, using small-angle X-ray scattering (SAXS) measurements.

The SAXS pattern obtained from the epoxy impregnated PBT film by using a pinhole-collimated incident beam is shown in Figure 2. It exhibits a narrow and intense equatorial streak, as expected of oriented microfibrils whose length is much larger than their width. The SAXS pattern obtained by using a slit-collimated incident beam, in the experimental geometry described in Figure 1, is shown in Figure 3. This pattern may be interpreted in terms of the structure in a cross-section plane perpendicular to the extrusion direction, since the assumptions of the derivations given in the preceding section are satisfied in this experiment:

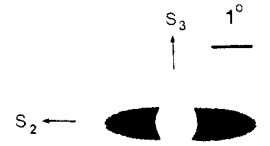

Figure 2. Small-angle scattering pattern from the epoxy-impregnated PBT film, obtained by using a pinhole-collimated incident beam.

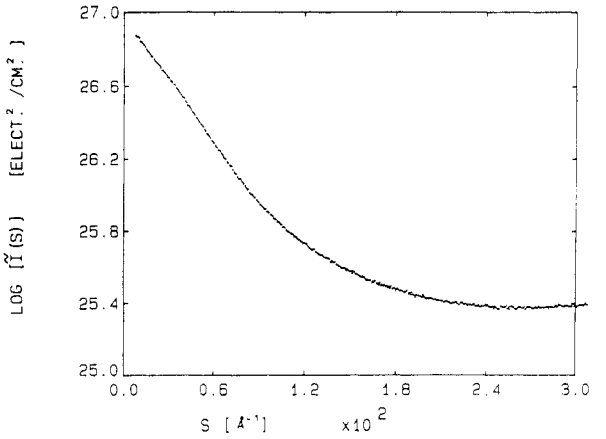

Figure 3. Small-angle scattering pattern from the epoxy-impregnated PBT film using a slit-collimated incident beam, after correction for parasitic scattering and detector sensitivity.

(a) The scattered radiation in the S_3 direction is of negligible intensity for values of S larger than about 0.005 Å^{-1}, as seen in Figure 2. The beam incident on the sample is of constant intensity up to a distance of 38 mm from its center point, which is equivalent to a value of S^* of about 0.046 Å^{-1}.

(b) By virtue of the continuous extrusion process by which the films were processed, the microstructure is expected to be homogeneous in the extrusion direction.

(c) The overall cylindrical symmetry of the microstructure has been verified by the equivalence of the wide-angle X-ray diffraction patterns obtained with the incident beam perpendicular to the front and edge faces of the film.

In order to interpret the structure in a cross sections of the microfibrils, it is assumed that the microfibrils are highly aligned parallel to the extrusion direction. This assumption is justified both by the SAXS pattern shown in Figure 2 and by the electron micrograph of a sample from the same film, shown in Figure 1 of ref 5. It is further assumed that the area fraction of the microfibrillar cross sections in a plane perpendicular to the extrusion direction equals the volume fraction of the microfibrillar PBT phase in the epoxy impregnated film.

In the SAXS pattern shown in Figure 3, the scattered intensity, $\tilde{I}(S)$, is a monotonically decreasing function of the scattering vector S. A plot of $S^3\tilde{I}(S)$ as a function of S^3, given in Figure 4, is linear at large values of the S. Thus,

$$\tilde{I}(S) = K_p/S^3 + F_1 \quad (24)$$

where K_p is the Porod constant for a two-phase system of constant densities and sharp interfaces in two dimensions,

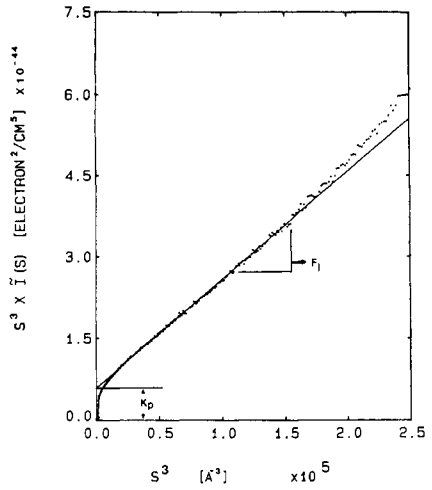

Figure 4. Experimental data plotted as $S^3\tilde{I}(S)$ versus S^3, to fit Porod's law.

as given in eq 16, and F_1 is the intensity scattered by small-scale density fluctuations in one or both phases,[19] which is assumed to be constant over the measured range of scattering angles. In this case F_1 reflects mostly the density fluctuations in the epoxy matrix. In further analysis, the value of F_1 determined from the slope in Figure 4 is subtracted from the measured intensity. The data points beyond $S = 0.026$ Å^{-1}, at which deviations from Porod's law appear in Figure 4, are exluded from further analysis.

The scattering invariant is calculated according to eq 8 by using the experimental data and asymptotic extrapolations at the extremities of the pattern. At low angles the Guinier approximation[20] is used. Beyond $S = 0.026$ Å^{-1} the scattering pattern is extrapolated by using Porod's law. The contribution to the total invariant from the low-angle extrapolation is less than 2%, and from the large angle extrapolation less than 10%.

The calculation of the scattering invariant, together with an independent measurement of the densities of the epoxy impregnated PBT film and the epoxy matrix, allows the determination of the volume fraction and density of the microfibrillar phase in the film. Under the assumption mentioned previously, that the area fraction of the microfibrillar phase in the cross section is equal to its volume fraction in the film, v_f, eq 8 and 12 written in terms of mass densities yield

$$\frac{Q}{L\lambda}\left(\frac{M_f}{Z_f N_{Av}}\right)^2 = \left(d_f - d_m \frac{Z_m M_f}{Z_f M_m}\right)^2 v_f(1 - v_f) \quad (25)$$

where M_f and M_m are the molecular weights and Z_f and Z_m are the number of electrons per repeat unit of PBT and the epoxy resin, respectively; d_f and d_m are the densities of the respective phases and N_{Av} is Avogadro's number. Under the assumption that all voids between the microfibrils have been filled by the epoxy resin, the film density, d, can be given as

$$d = d_f v_f + d_m v_m \quad (26)$$

From the chemical structure of both PBT and the epoxy resin we obtain $M_f = 266$, $Z_f = 136$, $M_m = 200$, and $Z_m = 109$. By measuring Q, d, and d_m, eq 25 and 26 can be solved for the density and volume fraction of the microfibrillar phase. From the Porod constant determined from the intercept in Figure 4, the interfacial contour length and the average diameter of the microfibrils are obtained. These measurements and results are summarized in Table I.

Table I
Analysis of the SAXS Pattern from Epoxy Impregnated PBT Film

Measurements	
scattering invariant	$Q = 1.1 \times 10^{39}$ electron^2/cm^4
Porod constant	$K_p = 5.9 \times 10^{43}$ electron^2/cm^5
film density	$d = 1.15$ g/cm^3
density of epoxy matrix	$d_m = 1.08$ g/cm^3
Results	
vol fraction of microfibrils	$v_f = 0.18$
density of microfibrils	$d_f = 1.46$ g/cm^3
interfacial length/unit vol	$C/A = 0.010$ Å^{-1}
av diameter of microfibrils	$\bar{D} = 71$ Å

The average microfibrillar diameter determined from the scattering pattern, 71 Å, is in good agreement with the observation by electron microscopy.[5] The calculated volume fraction, 0.18, indicates that volume shrinkage has occurred during the coagulation and/or the impregnation processes, as the weight fraction of PBT in the initial solution was about 0.06. The density of the microfibrils, calculated as 1.46 g/cm^3, is smaller than the density of the PBT crystal, estimated as 1.69 g/cm^3.[21] This indicates the existence of a significant number of imperfections within the individual microfibril. In a morphological study of PBT films, Minter et al.[22] observed regions of coherently packed PBT chains about 20 Å in width perpendicular to the chain axis, which increased to about 100 Å upon heat treatment. The microfibrils in the PBT films may as well be composed of smaller elements in which the chains are coherently packed, with the imperfections between these elements resulting in a lower overall density. These imperfections may be removed by heat treatment leading to a coherent packing of chains with a lateral dimension on the order of the microfibrillar width.

The size of the microfibrils has also been calculated by using the large-angle part of the scattering pattern (the "Porod region"). In order to obtain more information about the shape and packing of the cross sections of the microfibrils we attempt to simulate the complete scattering pattern, using more detailed models of the microfibrillar morphology.

The scattering pattern from a collection of particles having a well-defined shape can be calculated by using the Zernike–Prins equation[23]

$$\tilde{I}(S) = n|F^2(S)|G(s) \quad (27)$$

where $|F(S)^2|$ is the form factor of the individual scattering element, n is the density of particles in the system, and $G(S)$ is the interference factor, which for a centrosymmetric two-dimensional system is[17]

$$G(S) = 1 + n\int_0^\infty [g(R) - 1]J_0(2\pi SR)2\pi R \, dR \quad (28)$$

where $g(R)$ is the pair correlation function.

As a first approximation a model is proposed in which the microfibrils are long parallel cylinders, which appear in a cross-section plane as disks. The form factor of a disk of diameter D is[17]

$$|F^2(S)| = (\rho\pi D^2/4)J_1^2(\pi SD)/(\pi SD)^2 \quad (29)$$

where J_1 is the first-order Bessel function.

Considering polydispersity in the distribution of disk diameters, the expression for the scattered intensity can no longer be separated into a product of a form factor (intraparticle interference effects) and an interference factor (interparticle interference effects).[20] This can be overcome if the interparticle interference effects can be approximated by those of an equivalent monodisperse

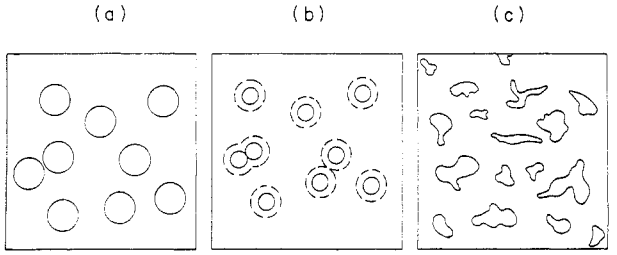

Figure 5. Schematic representation of the models used in simulation of the scattering pattern: (a) hard disks, (b) semipenetrable disks; (c) a random two-phase structure.

system of some "average particle". We will assume that the average particle is taken as one whose form factor equals the average form factor of the polydisperse system, defined as

$$\langle|F^2(S)|\rangle = \int_0^\infty P(D)|F^2(S,D)|\,dD \Big/ \int_0^\infty P(D)\,dD \qquad (30)$$

where $P(D)$ is the distribution function of disk diameters. Under this assumption the expression for the scattered intensity can be written as

$$\tilde{I}(S) = \langle|F^2(S)|\rangle G_e(S) \qquad (31)$$

where $G_e(S)$ is the interference factor prescribed for the equivalent monodisperse system.

A useful model for the interparticle interference in a cross section of a system composed of oriented fibrils is that of a hard-disk fluid.[24] This involves the assumption that the spatial average of the positions of the fibrillar cross sections equals the temporal average of the particle positions in the equivalent hard-disk fluid. The interference factor for a hard disk fluid may be calculated by applying the Percus Yevick approximation[25] to the Ornstein–Zernike equation.[26] Details of a convenient method for the evaluation of the interference factor for a hard-disk fluid have been given elsewhere.[24]

Three models are considered in the simulation of the scattering pattern from the epoxy impregnated PBT film. In the first two models the cross sections of the microfibrils are assumed to have a circular shape, and polydispersity in the distribution of diameters is considered. Thus in these models the form factor is calculated by using eq 30 and a Gausian distribution of disk diameters, for which $\langle D^2\rangle/\langle D\rangle$ = 71 Å, as calculated from the analysis of the Porod region. A standard deviation of 20 Å is used, as no form factor peaks are apparent in the scattering pattern. The two models differ in the way in which the relative positions of the microfibrils within the cross section are taken into account (i.e., in the way the interference factor $G_e(S)$ is calculated). In the first model, the spatial average of the positions of the microfibrils is approximated as the temporal average of the positions of disks in a two-dimensional fluid of impenetrable hard disks. The interference factor is evaluated by using an area fraction of 0.18, which is equal to the calculated volume fraction of microfibrils. This model is thus referred to as a "hard-disk" model and is shown schematically in Figure 5a.

In the second model, the distance between the centers of the microfibrils is allowed to have a value smaller than the average diameter of the microfibrils, as may occur in a cross section of a junction between two microfibrils. The interference factor is approximated as that of a hard-disk fluid having the same number of disks per unit area as in the previous model but with a smaller apparent diameter, hence a smaller apparent area fraction. This allows the minimal distance between the centers of the disks to be less than the average disk diameter, as shown in Figure 5b, and may thus simulate the cross-section of a junction between microfibrils. The interference factor evaluated for this model is thus similar to that of a two-dimensional fluid of semipenetrable disks and will be referred to as such. This should not be taken to imply that the microfibrils can penetrate each other.

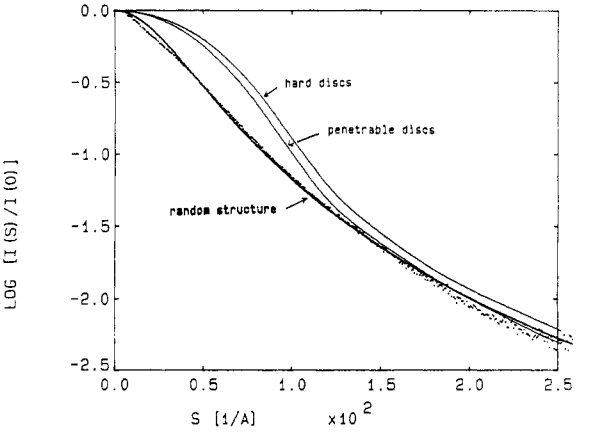

Figure 6. Comparison of the experimentally measured scattering pattern with the simulations obtained by using the structural models described in Figure 5.

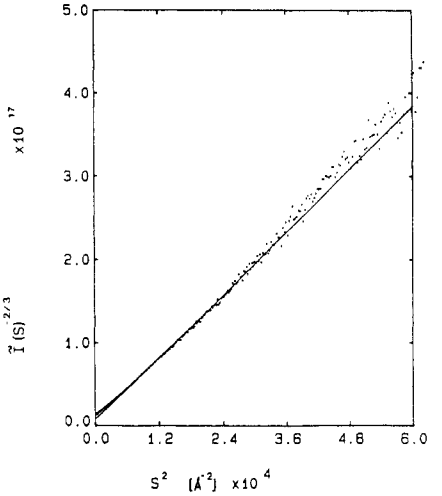

Figure 7. Experimental data plotted as $\tilde{I}(S)^{-2/3}$ versus S^2, to fit eq 23.

As a third model, the structure in the cross section of the film is simulated as a random two-phase structure. Such structure is shown schematically in Figure 5c. In this case the scattering pattern is simulated by using eq 23.

The three simulated patterns are compared with the experimental measurement in Figure 6. The intensity at zero angle is set to be equal for the measurement and simulations. The hard-disk model fits the experimental measurement poorly. A better fit at the large angle part of the scattering pattern is obtained with the semipenetrable disk model, using an apparent hard-disk diameter $D_a = 0.8\bar{D}$ in the calculation of the interference factor. Both models fail in the smaller angle part of the scattering pattern, where the higher intensities predicted by these models are a direct consequence of the spatial correlations between the hard or semipenetrable disks.

A good fit of the experimental data is obtained with the random two-phase structure model in the entire experimentally accessible range. It is obtained by using a correlation length of 36 Å, which is estimated from a plot of $\tilde{I}(S)^{-2/3}$ as a function of S^2, shown in Figure 7. This suggests that the cross sections of the microfibrils have irregular shapes. The average cord length of the micro-

fibrillar cross sections, l_f, as defined by Porod,[13] is given by

$$l_f = l_c/(1 - v_f) \tag{32}$$

The value of l_f thus calculated, 44 Å, is smaller than the observed dimension of the microfibrils. In addition the interfacial contour length per unit area calculated from the correlation length by eq 23, 0.013 Å^{-1}, is larger than that calculated from Porod's law. This may reflect the fact that in using Porod's law the information is obtained from the large-angle part of the scattering pattern, whereas eq 23 is fit to the entire pattern, giving more weight to the smaller angle region.

Conclusions

1. The scattering pattern obtained from a system composed of oriented fibrils by using a slit-collimated incident beam can yield information about the structure in a cross-section plane perpendicular to the direction of orientation. Scattering laws pertaining to a two-dimensional system are derived, in analogy to the commonly used ones for a three-dimensional system.

2. The network of oriented microfibrils which is formed in the coagulation stage of the spinning process of PBT films can be characterized by SAXS measurements. The average diameter of the microfibrils is measured as 71 Å, and their density is 1.46 g/cm^3, somewhat lower than the density of PBT crystals (1.69 g/cm^3) due to imperfections within the microfibrils.

3. Three models for the structure in the cross section perpendicular to the microfibril direction are used in simulation of the scattering pattern: hard disks, semipenetrable disks, and a random two-phase structure. Of these, the random structure model fits the experimental data best. This suggests that the cross sections of the microfibrils have irregular shapes.

Acknowledgment. Financial support from the U.S. Air Force, through Grants F33615-82-K5068 and AFOSR-85-2075, is gratefully acknowledged. Use of the facilities of the NSF sponsored Materials Research Laboratory at the University of Massachusetts is appreciated. We thank Dr. C. G. Vonk for helpful discussions and Prof. W. Ruland for communication of an unpublished report.

Appendix

In order to calculate $\int_0^\infty x^p J_0(x)\,dx$, define

$$I_0(\lambda) = \int_0^\infty e^{-\lambda x} J_0(x)\,dx \tag{A.1}$$

then[18]

$$I_0(\lambda) = (1 + \lambda^2)^{-1/2} \tag{A.2}$$

and

$$\int_0^\infty x^p J_0(x)\,dx = (-1)^p \left[\frac{d^p I_0(x)}{d\lambda^p}\right]_{\lambda=0} \tag{A.3}$$

Taking derivatives of (A.2) and substituting in (A.3) yield

$$\int_0^\infty x J_0(x)\,dx = 0 \qquad \int_0^\infty x^2 J_0(x)\,dx = -1$$
$$\int_0^\infty x^3 J_0(x)\,dx = 0 \tag{A.4}$$

Registry No. PBT, 69794-31-6.

References and Notes

(1) Hearle, J. W. S., Peters, R. H., Eds. *Fiber Science*; Butterworth: London, 1963.
(2) Parades, E.; Fischer, E. W. *Makromol. Chem.* **1979**, *180*, 2707.
(3) Brown, H. R.; Kramer, E. J. *J. Makromol. Sci., Macromol. Phys.* **1981**, *19*, 487.
(4) Rudall, K. M.; Kenchington, W. *Biol. Rev.* **1973**, *49*, 597.
(5) Cohen, Y.; Thomas, E. L. *Macromolecules*, preceding paper in this issue.
(6) Lee, C. C.; Chu, S. G.; Berry, G. C. *J. Polym. Sci., Polym. Phys. Ed.* **1983**, *21*, 1573.
(7) Wolfe, J. F.; Loo, B. H.; Arnold, F. E. *Macromolecules* **1981**, *14*, 915.
(8) Cohen, Y.; Thomas, E. L. *Polym. Eng. Sci.* **1985**, *25*, 1093.
(9) Kratky, O.; Pilz, I.; Schmitz, P. J. *J. Colloid Interface Sci.* **1966**, *21*, 24.
(10) Perret, A.; Ruland, W. *J. Appl. Cryst.* **1969**, *2*, 209.
(11) Dettenmaier, M. *Adv. Polym. Sci.* **1983**, *52/53*, 57.
(12) Ruland, W., private communication.
(13) Porod, G. *Kolloid-Z.* **1951**, *124*, 83; **1952**, *125*, 51; **1952**, *125*, 108.
(14) Debye, P.; Bueche, A. M. *J. Appl. Phys.* **1949**, *20*, 518.
(15) Debye, P.; Anderson, H. R.; Brumberger, H. *J. Appl. Phys.* **1957**, *28*, 679.
(16) Kirste, R.; Porod, G. *Kolloid Z.-Z. Polym.* **1962**, *184*, 1.
(17) Oster, G.; Riley, D. P. *Acta Crystallogr.* **1953**, *5*, 272.
(18) Gradshteyn, I. S.; Rhyzik, I. M. *Tables of Integrals, Series and Sums*; Academic: New York, 1980.
(19) Ruland, W. *J. Appl. Cryst.* **1971**, *4*, 70.
(20) Guinier, A.; Fournet, G. *Small-Angle Scattering of X-Rays*; Wiley: New York, 1955.
(21) Roche, E. J.; Takahashi, T.; Thomas, E. L. In *Fiber Diffraction Methods*; French, A. D., Gardner, K. H., Eds.; ACS Symposium Series 141; American Chemical Society: Washington, DC, 1980; 303.
(22) Minter, J. R.; Shimamura, K.; Thomas, E. L. *J. Mater. Sci.* **1981**, *16*, 3303.
(23) Zernike, F.; Prins, J. A. *Z. Phys.* **1927**, *41*, 184.
(24) Cohen, Y.; Thomas, E. L. *J. Polym. Sci., Polym. Phys. Ed.* **1987**, *25*, 1607.
(25) Percus, J. K.; Yevick, G. J. *Phys. Rev.* **1958**, *110*, 1.
(26) Ornstein, L. S.; Zernicke, F. *Proc. Akad. Sci. (Amsterdam)* **1914**, *17*, 793.